PROCEEDINGS OF SPIE

SPIEDigitalLibrary.org/conference-proceedings-of-spie

Improving accuracy of image-to-physical laparoscopic liver registration via reconstruction of intrahepatic pressure changes from abdominal insufflation

Heiselman, Jon, Richey, Winona, Taylor, Shannon, Miga, Michael

Jon S. Heiselman, Winona L. Richey, Shannon L. Taylor, Michael I. Miga, "Improving accuracy of image-to-physical laparoscopic liver registration via reconstruction of intrahepatic pressure changes from abdominal insufflation," Proc. SPIE 11598, Medical Imaging 2021: Image-Guided Procedures, Robotic Interventions, and Modeling, 115980W (15 February 2021); doi: 10.1117/12.2582155

SPIE.

Event: SPIE Medical Imaging, 2021, Online Only

Improving accuracy of image-to-physical laparoscopic liver registration via reconstruction of intrahepatic pressure changes from abdominal insufflation

Jon S. Heiselman[1,2], Winona L. Richey[1,2], Shannon L. Taylor[1,2] and Michael I. Miga[1,2]

[1]Department of Biomedical Engineering, Vanderbilt University, Nashville, TN
[2]Vanderbilt Institute for Surgery and Engineering, Vanderbilt University, Nashville, TN

ABSTRACT

During laparoscopic surgery, insufflation introduces significant deformations to the liver through reshaping the abdominal cavity. Additionally, insufflation is associated with elevation of portal and hepatic venous pressures causing hemodynamic changes that may cause swelling or engorgement of the liver. Current methods for elastic soft tissue registration cannot account for these secondary effects, which have yet remained largely neglected. This paper presents preliminary work towards modeling these intraoperative physiological changes caused by insufflation to improve the accuracy of image-to-physical registration during laparoscopic procedures. Spatially localized modes of internal pressure-driven deformations are introduced to allow reconstruction of intraoperative changes to intrahepatic pressure gradients during registration. A pilot experiment was performed in one sheep to measure volumetric tissue changes induced by insufflation. Liver volume increased by 6.3 ± 0.7% between insufflated and preoperative states, according to three independent raters. Registrations were also performed between organ states, utilizing: (1) rigid registration, (2) deformable registration based on application of external forces to the organ, and (3) the same deformable registration extended to incorporate displacements driven by changes to intrahepatic pressure gradients. Target registration error (TRE) decreased from 15.2 ± 3.2 mm with rigid registration to 5.0 ± 1.9 mm with reconstruction of external boundary forces. When incorporating internal pressure changes, TRE further decreased to 3.0 ± 1.2 mm. Additional analysis comparing a pure scaling approach with the proposed mechanics-based method to account for volume change demonstrated that the method incorporating intrahepatic pressure changes leads to more accurate image-to-physical registrations between the preoperative and insufflated liver.

Keywords: Registration, laparoscopy, image guidance, liver, insufflation, volume, pressure

1. INTRODUCTION

Insufflation is a defining characteristic of laparoscopic surgery that imparts significant intraoperative changes to the abdominal cavity by elevating intra-abdominal pressure. With regard to the liver, insufflative pressurization causes reshaping of the abdominal cavity that distends the ventral wall and diaphragm. These motions are directly transduced to the liver by the falciform and triangular ligaments. In addition, elevation of ambient pressure surrounding the organ imparts a distributed compressive force to the liver. Consequently, existing approaches for laparoscopic image-to-physical registration of the liver mainly propose the use of external force constraints on linear elastic mechanical models of the organ to improve the accuracy of deformable soft tissue registration[1–4].

However, changes in organ volume can occur between preoperative and intraoperative stages. An animal study by Kenngott *et al*. recently showed significant decreases in total liver volume exceeding 7% and 13%, respectively, between the native preoperative state of the organ and open and laparoscopic intraoperative surgical states[5]. Although human studies are more limited due to the availability of intraoperative imaging, those that have reported organ volumes indicate greater variance in volume change. For example, Heizmann *et al*. showed volume changes ranging from –12.6% to +24.0% between preoperative and intraoperative CT imaging during open liver surgery. This variation could be caused by many factors that may influence liver

Medical Imaging 2021: Image-Guided Procedures, Robotic Interventions, and Modeling,
edited by Cristian A. Linte, Jeffrey H. Siewerdsen, Proc. of SPIE Vol. 11598, 115980W

volume. For example, innate variations depending on time of day have been observed, with average peak-to-peak difference of 17% between morning and early afternoon[6]. When performing elastic registration, accounting for these volume changes can become problematic due to limitations on strain energy and the consideration that soft tissue is often modeled as nearly incompressible. Though energy minimization methods are commonly employed for solving registration problems[1–3,7–10], a major limitation of these methods is their inability to represent volumetric change without incurring large amounts of strain energy throughout the domain. Volumetric strains that are responsible for volume change incur large energetic penalties and consequently are also minimized in effect. While this minimization of volumetric distortion is often a beneficial constraint, the capacity to model actual changes in organ volume subsequently becomes debilitated, especially when strain energy is used for regularizing a predicted deformation field.

During laparoscopy, volume changes may occur due to insufflation directly imparting compressive forces on the liver. Additionally, laparoscopic insufflation induces other physiological hemodynamic changes in the liver through elevation of venous pressures. Measurements from porcine insufflation studies have indicated that blood pressure in the portal vein and inferior vena cava increase one-to-one with insufflation pressure[11], while the pressure of the hepatic artery remains approximately constant throughout insufflation[12]. The additional venous resistance may cause a change in pressure gradient across the liver that forces additional blood volume into the hepatic parenchyma, leading to engorgement of the liver and increased liver volume. Furthermore, when assuming elastic tissue behavior, physiological sources of volume change that occur during laparoscopy may cause additional error when attempting to register liver anatomy between preoperative and intraoperative organ states, due to the origination of internal forces that are not fully captured by purely elastic responses to surface motions. In order to account for volumetric changes in the liver during image-to-physical registration, additional modeling efforts are required to more accurately represent deformation under these conditions where relative change in organ volume may occur. In this preliminary work, we present an animal study to identify the volumetric effect of insufflation on the liver and introduce an algorithmic approach that incorporates intraoperative changes to intrahepatic vascular pressures with a reconstructive framework for compensating soft tissue deformation during image-to-physical registration of the liver.

2. METHODS

2.1 Reconstruction of Hemodynamic Pressure Changes

A biphasic porous media model is used to simulate changes in elastic volume and displacements in response to changes in intrahepatic pressure gradients. These equations consist of the conventional Navier-Cauchy equations for linear elasticity coupled to a fully saturated and steady state fluid phase component[13]:

$$\mu\nabla^2 u + (\lambda + \mu)\nabla(\nabla \cdot u) - \nabla p = 0 \quad (1)$$

$$\nabla \cdot (-\kappa\nabla p) + k_t p = 0 \quad (2)$$

where u is the displacement vector, p is the interstitial pressure of fluid within the parenchyma, μ and λ are the Lamé parameters, κ is hydraulic conductivity, and k_t is tissue permeability. When $k_t = 0$, fluid is allowed to redistribute within the organ but is fully conserved. When $k_t > 0$, elevated pressures are allowed to drive additional fluid into the tissue to cause a swelling effect.

Engorgement caused by changes in vascular pressures across the hepatic inflow and outflow are compensated by simulating and reconstructing intraoperative changes to the intrahepatic pressure gradients to match the observed intraoperative displacements of the organ surface. This task is accomplished by pre-computing a series of pressure-displacement modes that are locally regionalized within the liver. First, a tetrahedral finite element mesh of the liver is constructed from an image volume in its native state within the closed abdomen. Then, *k*-means clustering is used to select *k* uniformly sampled reconstruction points from all mesh vertices within the domain (Figure 1a). For analysis, the number of reconstruction points was varied between 0 and 75

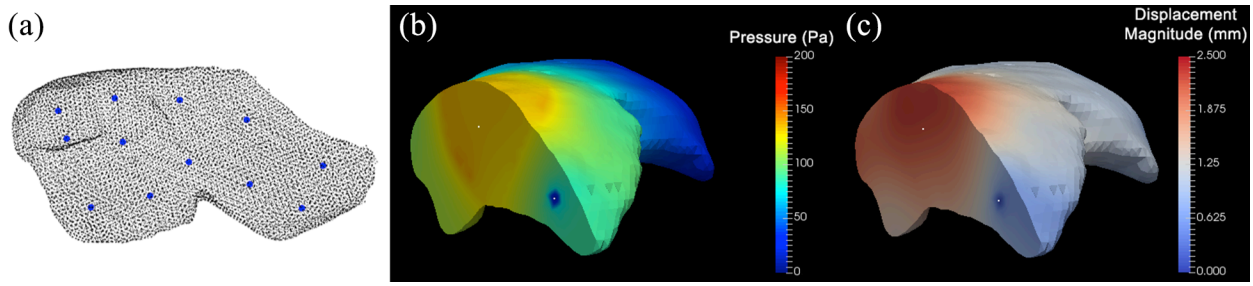

Figure 1. (a) Pressure reconstruction points sampled throughout the liver mesh; each reconstruction point serves as a virtual pressure source for reconstructing intraoperative intrahepatic pressure gradients. (b) Relaxed pressure response for one active reconstruction mode. (c) Displacement response for pressure mode in (b).

in increments of 15. Second, for each reconstruction point, (1) and (2) are solved using the Galerkin weighted residual method with boundary conditions of pressure at the active reconstruction point set to 1 kPa, and displacements and pressures of all other reconstruction points set to zero. All other vertices adopt the natural zero-gradient Neumann boundary condition. Third, each response is relaxed using the Saint-Venant principle to diffuse the point responses from pressure and displacement onto the Voronoi region of the active k-means cluster using the method of Heiselman et al.[8] Finally, the relaxed displacement modes (Figure 1b, 1c) are incorporated into the linearized iterative boundary reconstruction method[8] with 45 control points on the organ surface, which reconstructs external forces applied to the organ between an initial and deformed state. This process was done with Lamé parameters corresponding to a Young modulus of 2100 kPa and Poisson ratio of 0.45, $\kappa = 1.0 \times 10^{-10}$ $m^4s^{-1}Pa^{-1}$, and was repeated for varying tissue permeability. A value of $k_t = 0$ $m^2s^{-1}Pa^{-1}$ was first introduced to model fully conserved and localized internal redistribution of fluid within the organ (CPR, conserved pressure reconstruction). Separately, displacement mode response matrices corresponding to $k_t = 1.0 \times 10^{-6}$ and $k_t = 1.0 \times 10^{-5}$ $m^2s^{-1}Pa^{-1}$ were concatenated and incorporated into the reconstruction method to model permeable tissue that allows a pressure-dependent transfer of fluid that drives local volume changes (permeable pressure reconstruction, PPR).

Briefly, the linearized iterative boundary reconstruction (BR) method produces a localized basis of displacement mode responses J_u that decompose external forces acting on the organ so that a linear combination of mode responses parameterizes the configuration of external loading on the organ. The method operates by defining a model-data error term $\boldsymbol{p}_i$ for each intraoperative data point,

$$\boldsymbol{p}_i = \boldsymbol{y}_i - C_i(R(\boldsymbol{x}_0 - \overline{\boldsymbol{x}}_0 + J_u\boldsymbol{\alpha}) + \boldsymbol{\tau} + \overline{\boldsymbol{x}}_0) \tag{3}$$

where $\boldsymbol{y}_i$ is the position of the observed data point, and the deformed model is defined by the undeformed mesh node positions $\boldsymbol{x}_0$, the mesh centroid $\overline{\boldsymbol{x}}_0$, the correspondence operator C_i, and parameters consisting of a vector of mode weights $\boldsymbol{\alpha}$, a translation vector $\boldsymbol{\tau}$, and rotation vector $\boldsymbol{\theta}$ that encodes the rotation matrix R. The parameters are then optimized by minimizing the objective function

$$\Omega(\boldsymbol{\alpha}, \boldsymbol{\tau}, \boldsymbol{\theta}) = \sum_F \frac{w_F}{N_F} \sum_{i=1}^{N_F} f(\boldsymbol{p}_i)^2 + w_E \overline{U}^2 \tag{4}$$

where N_F is the number of data points within an anatomical feature used in registration, w_F is the weight of the feature, $f(\boldsymbol{p}_i)$ is the projected error to the feature, w_E is the weight of energy regularization, and $\overline{U}$ is the strain energy density. When incorporating pressure-driven modes of deformation, the response matrix J_u and weight vector $\boldsymbol{\alpha}$ are extended. However, the pressure-driven modes are excluded from strain energy computation to allow for reconstruction of hemodynamic pressure changes without saturating the energy of deformation. It should be noted that because the sign of each element of $\boldsymbol{\alpha}$ is unrestricted, volume shrinkage

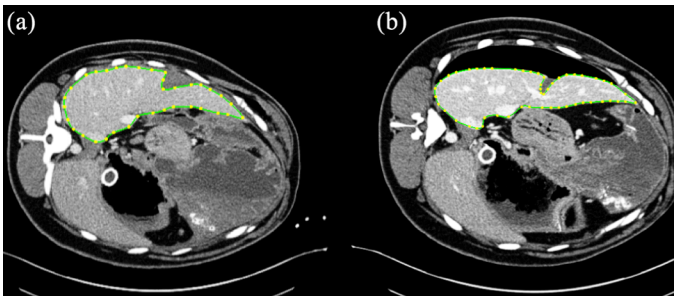

Figure 2. Contrast-enhanced CT images of sheep liver in (a) closed abdomen, and (b) insufflated abdomen.

caused by pressure decreases relative to the resting pressure distribution, for example due to bleeding or other effects, can also be represented by these deformation modes.

The mechanics-based approaches for compensating internal pressures and volume changes were also compared to a non-mechanical extension of the BR method that incorporates an isotropic volumetric scaling term by adjusting the model-data error term to

$$\boldsymbol{p}_i = \boldsymbol{y}_i - C_i(R\sigma I(\boldsymbol{x}_0 - \overline{\boldsymbol{x}}_0 + J_u\boldsymbol{\alpha}) + \boldsymbol{\tau} + \overline{\boldsymbol{x}}_0) \quad (5)$$

where σ is a scale factor and I is the identity matrix. When isotropic scaling (IS) was included in registration, the scale factor σ was also optimized as a parameter of the objective function $\Omega(\boldsymbol{\alpha}, \boldsymbol{\tau}, \boldsymbol{\theta}, \sigma)$.

2.2 Animal Data

One Suffolk sheep was included in this pilot study following all applicable international, national, and institutional guidelines and ethical standards for the care and use of animals. First, four biopsy clips were implanted percutaneously in the liver to serve as validation targets. Then, contrast-enhanced CT images of the sheep liver were obtained in the closed abdomen (Figure 2a) and insufflated abdomen (Figure 2b). These images record the change in liver volume, liver shape, and displacement of biopsy clip targets between native and insufflated states of the organ. Three independent raters were instructed to segment the liver from both CT images, and registrations were performed to align the initial anatomy from the closed image with the liver surface from the insufflated scan. Subsurface target registration error (TRE) was measured by the Euclidean distance between the predicted and actual positions of the four biopsy clip targets in the insufflated organ volume. Volume error was computed as the percent error of the volume of the registered model relative to the ground truth volume of the insufflated liver. TRE was measured after semiautomatic rigid registration[14], after the linearized iterative boundary reconstruction method (BR), after boundary reconstruction with isotropic scaling (BR + IS), after boundary reconstruction and conserved pressure reconstruction (BR + CPR), after boundary and conserved pressure reconstruction with isotropic scaling (BR + CPR + IS), and after boundary reconstruction and permeable pressure reconstruction (BR + PPR). These registrations were repeated using each of the segmentations from the three raters to yield 12 total target samples per trial.

3. RESULTS

Across all segmentation raters, the volume of the liver in the closed abdomen was 855 ± 13 mL. The volume of the liver during insufflation was 908 ± 9 mL, representing a 6.3 ± 0.7% increase in liver volume that was found to be statistically significant (p = 0.004, paired t-test). The volume of each segmentation is shown in Table 1.

Segmentation	Closed Liver Volume (mL)	Insufflated Liver Volume (mL)	Volume Increase (%)
1	840	898	+7.0
2	864	911	+5.5
3	861	916	+6.4
Average	**855 ± 13**	**908 ± 9**	**+6.3 ± 0.7**

Table 1. Closed and insufflated liver volumes segmented by each independent annotator.

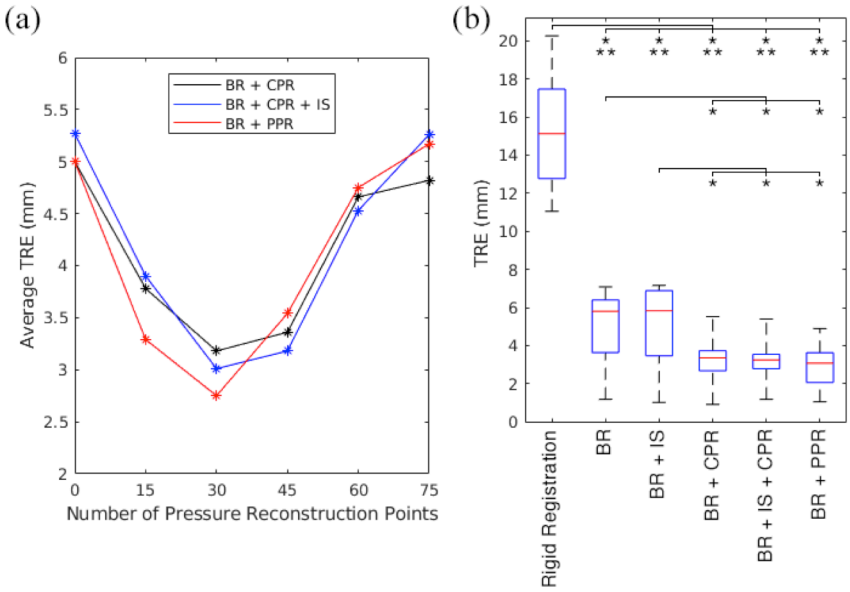

Figure 3. (a) Average TRE plotted against the number of points selected for localized modes of internal pressure reconstruction, using organ models from segmentation 1. (b) Target registration errors for each registration, showing combined results from organ models derived from all three segmentations. Differences compared with paired t-test (⁂ indicates $p < 0.001$; * indicates $p < 0.05$).

Target	TRE (mm), Rigid	TRE (mm), BR	TRE (mm), BR + IS	TRE (mm), BR + CPR	TRE (mm), BR + CPR + IS	TRE (mm), BR + PPR
1	15.0 ± 0.5	6.0 ± 0.7	6.3 ± 0.8	4.0 ± 1.3	4.0 ± 1.2	3.8 ± 1.0
2	11.1 ± 0.1	2.0 ± 0.8	1.7 ± 0.7	2.7 ± 1.6	2.6 ± 1.3	3.3 ± 2.0
3	19.8 ± 0.4	6.6 ± 0.5	7.1 ± 0.1	2.9 ± 0.4	2.9 ± 0.3	2.1 ± 0.5
4	14.9 ± 0.5	5.4 ± 0.8	5.3 ± 0.9	3.8 ± 1.5	3.8 ± 1.6	2.8 ± 0.6
Average	**15.2 ± 3.2**	**5.0 ± 1.9**	**5.1 ± 2.2**	**3.4 ± 1.2**	**3.3 ± 1.2**	**3.0 ± 1.2**

Table 2. TRE of the four biopsy clip targets for rigid registration, linearized iterative boundary reconstruction (BR), boundary reconstruction with isotropic scaling (BR + IS), and boundary reconstruction with the proposed localized conserved pressure reconstruction (CPR) and permeable pressure reconstruction (PPR) modes across models derived from the three independent organ segmentations.

Figure 3a shows a characterization of the relationship between TRE and the number of pressure reconstruction points, demonstrating that increasing the number of internal pressure modes provides an improvement over external reconstruction of forces until further expanding the number of parameters exceeds the ability for a solution to be adequately determined from the data provided to the reconstruction. With these curves suggesting that 30 pressure reconstruction points offers an optimal balance of reconstructive resolution, this number was used for all subsequent pressure-reconstructive registrations.

Segmentation	Volume Error (%), Rigid	Volume Error (%), BR	Volume Error (%), BR + IS	Volume Error (%), BR + CPR	Volume Error (%), BR + CPR + IS	Volume Error (%), BR + PPR
1	6.2	6.3	3.9	7.0	6.1	5.8
2	5.2	5.3	3.9	5.1	6.0	3.1
3	6.0	5.6	4.5	5.5	5.2	4.9
Average	**5.9 ± 0.6**	**5.8 ± 0.5**	**4.1 ± 0.4**	**5.9 ± 1.0**	**5.8 ± 0.5**	**4.6 ± 1.4**

Table 3. Volume errors after registration of organ models derived from the segmentations of each annotator.

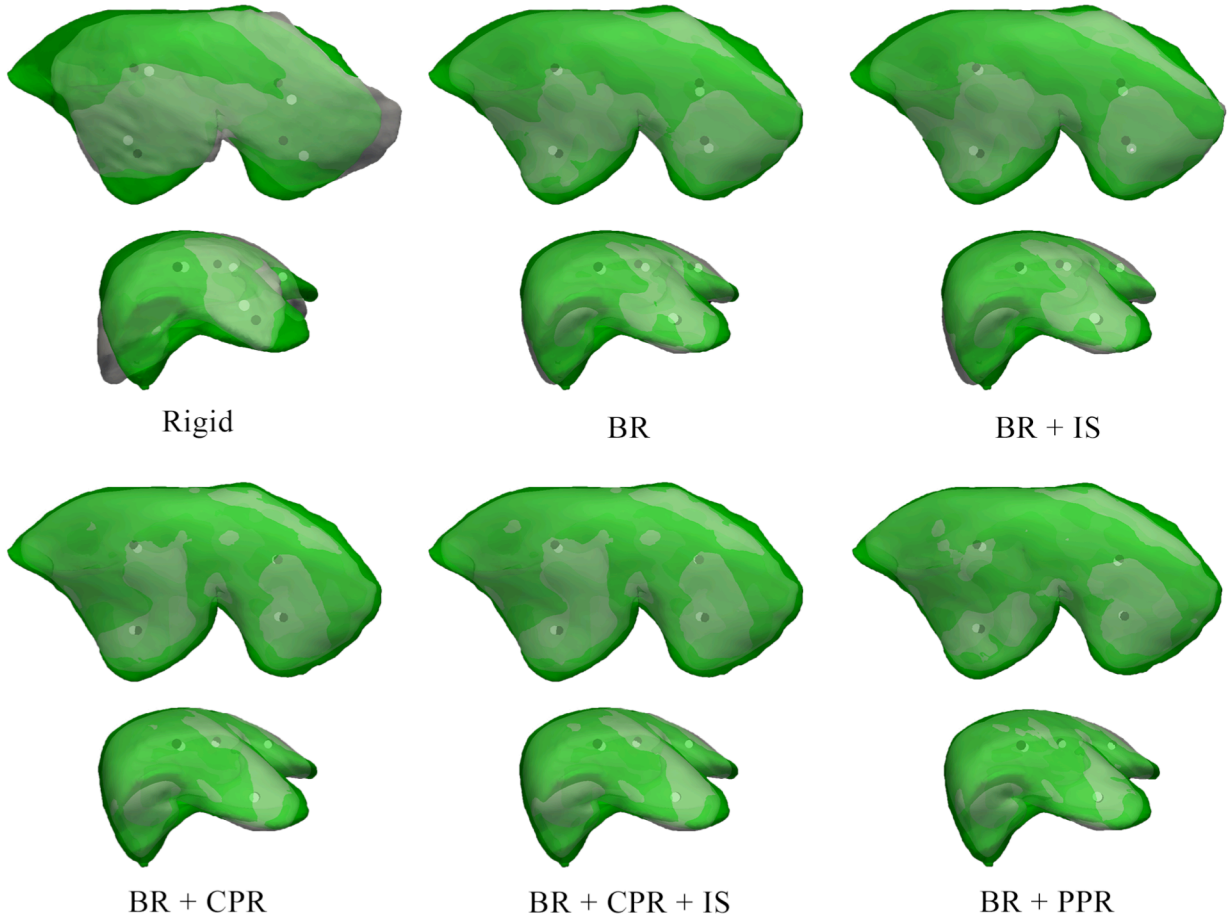

Figure 4. Registration alignments showing ground truth insufflated liver (green) and biopsy clip positions (black) compared to registered preoperative liver (gray) and predicted biopsy clip positions (white) for rigid registration (top left), linearized iterative boundary reconstruction (top center), boundary reconstruction with isotropic scaling (top right), boundary plus conserved pressure reconstruction (bottom left), boundary plus conserved pressure reconstruction with isotropic scaling (bottom center), and boundary plus permeable pressure reconstruction (bottom right).

In Figure 3b, TRE of the biopsy clip targets are shown for each registration trial. Quantitative values of TRE are reported in Table 2, and registered volume errors are reported in Table 3. Figure 4 shows the registered livers and positions of the four implanted biopsy clip targets after each registration.

4. DISCUSSION

The boundary reconstruction method for external forces reduces average TRE from 15.2 ± 3.2 mm after rigid registration to 5.0 ± 1.9 mm after deformable correction, representing a threefold improvement in accuracy using this baseline method. While significantly more accurate, the boundary reconstruction method was not able to effectively compensate for the change in volume of the organ, providing nearly identical volume error as rigid registration. Interestingly, when isotropic scaling was added to the boundary reconstruction, volume error decreased but accuracy did not improve. This observation suggests that this non-mechanical form of volume scaling does not correctly communicate volume change into realistic displacements.

When conserved pressure modes are incorporated into the boundary reconstruction, TRE further decreases to 3.4 ± 1.2 mm. Although this addition allows redistribution of pressures and exchange of fluid across regions of the liver to better match intrahepatic responses to insufflation, conservation of flow cannot produce net volume change and therefore cannot effectively compensate for it. However, this approach of conserved redistribution of internal pressure gradients still provides significantly improved accuracy over the baseline boundary reconstruction method, suggesting that insufflation may cause internal physiological changes to the liver that cannot be fully compensated by application of external forces.

Finally, when tissue permeability is added, TRE further decreases to 3.0 ± 1.2 mm, representing a 40% improvement on the baseline boundary reconstruction method, and more than a fivefold improvement over rigid registration. Moreover, partial volume compensation is observed through a decrease in volume error. This gain suggests that by incorporating these adjustable perfusion terms within the deformation model, internal vascular changes can be more effectively captured by the registration. Remarkably, optimization of these internal pressure modes is possible from data provided only on the organ surface. Although these registrations were performed between full organ surface segmentations, future work will investigate accuracy when registration is performed on sparse data typically achievable in the operating room without the use of intraoperative CT. Additionally, further studies are needed on larger sample sizes to validate the method on more diverse samples of liver change in response to laparoscopic insufflation.

5. CONCLUSION

This work introduces a preliminary animal experiment and methodological advancement that aims to compensate for intrahepatic physiological changes to the liver caused by insufflation during laparoscopic image-to-physical registration. While many existing methods attempt to compensate for purely elastic effects, this work introduces a preliminary method to more accurately model intraoperative changes in organ pressure using a biphasic model to reconstruct internal vascular-driven changes experienced by the liver during laparoscopy. An animal experiment was performed to measure the impact of laparoscopic insufflation on registration accuracy. This work finds that combining localized modes of tissue swelling caused by changes in internal organ pressure gradients with a reconstruction method of external organ forces can significantly improve the accuracy of image-to-physical registration during laparoscopy.

ACKNOWLEDGMENTS

This work has been supported the NIH grants NIBIB-R01EB027498, NIBIB-T32EB021937, and NCI-R01CA162477.

REFERENCES

[1] Heiselman, J. S., Clements, L. W., Collins, J. A., Weis, J. A., Simpson, A. L., Geevarghese, S. K., Kingham, T. P., Jarnagin, W. R. and Miga, M. I., "Characterization and correction of soft tissue deformation in laparoscopic image-guided liver surgery," J. Med. Imaging **5**(2), 021203 (2018).

[2] Plantefève, R., Peterlik, I., Haouchine, N. and Cotin, S., "Patient-specific biomechanical modeling for guidance during minimally-invasive hepatic surgery," Ann. Biomed. Eng. **44**(1), 139–153 (2016).
[3] Modrzejewski, R., Collins, T., Seeliger, B., Bartoli, A., Hostettler, A. and Marescaux, J., "An in vivo porcine dataset and evaluation methodology to measure soft-body laparoscopic liver registration accuracy with an extended algorithm that handles collisions," Int. J. Comput. Assist. Radiol. Surg. **14**(7), 1237–1245 (2019).
[4] Özgür, E., Koo, B., Le Roy, B., Buc, E. and Bartoli, A., "Preoperative liver registration for augmented monocular laparoscopy using backward–forward biomechanical simulation," Int. J. Comput. Assist. Radiol. Surg. **13**(10), 1629–1640 (2018).
[5] Kenngott, H. G., Nickel, F., Preukschas, A. A., Wagner, M., Bihani, S., Özmen, E., Wise, P. A., Bellemann, N., Sommer, C. M., Norajitra, T., Graser, B., Stock, C., Nolden, M., Mehrabi, A. and Müller-Stich, B. P., "Effects of laparoscopy, laparotomy, and respiratory phase on liver volume in a live porcine model for liver resection," Surg. Endosc. **in press** (2021).
[6] Leung, N. W. Y., Farrant, P. and Peters, T. J., "Liver volume measurement by ultrasonography in normal subjects and alcoholic patients," J. Hepatol. **2**, 157–164 (1986).
[7] Rucker, D. C., Wu, Y., Clements, L., Ondrake, J., Pheiffer, T., Simpson, A., Jarnagin, W. and Miga, M., "A mechanics-based nonrigid registration method for liver surgery using sparse intraoperative data.," IEEE Trans. Med. Imaging **33**(1), 147–158 (2014).
[8] Heiselman, J. S., Jarnagin, W. R. and Miga, M. I., "Intraoperative correction of liver deformation using sparse surface and vascular features via linearized iterative boundary reconstruction," IEEE Trans. Med. Imaging **39**(6), 2223–2234 (2020).
[9] Suwelack, S., Röhl, S., Bodenstedt, S., Reichard, D., Dillmann, R., dos Santos, T., Maier-Hein, L., Wagner, M., Wünscher, J., Kenngott, H., Müller, B. P. and Speidel, S., "Physics-based shape matching for intraoperative image guidance," Med. Phys. **41**, 1–12 (2014).
[10] Peterlík, I., Courtecuisse, H., Rohling, R., Abolmaesumi, P., Nguan, C., Cotin, S. and Salcudean, S., "Fast elastic registration of soft tissues under large deformations," Med. Image Anal. **45**, 24–40 (2018).
[11] Liem, T., Applebaum, H. and Herzberger, B., "Hemodynamic and ventilatory effects of abdominal CO2 insufflation at various pressures in the young swine," J. Pediatr. Surg. **29**(8), 966–969 (1994).
[12] Antoniou, E. A., Kairi, E. V. I., Margonis, G. A., Andreatos, N., Sasaki, K., Damaskos, C., Garmpis, N., Samaha, M., Argyra, E., Polymeneas, G., Weiss, M. J., Pawlik, T. M., Voros, D. and Kouraklis, G., "Effect of increased intra-abdominal pressure on liver histology and hemodynamics: an experimental study," In Vivo. **32**(1), 85–91 (2018).
[13] Paulsen, K. D., Miga, M. I., Kennedy, F. E., Jack Hoopes, P., Hartov, A. and Roberts, D. W., "A computational model for tracking subsurface tissue deformation during stereotactic neurosurgery," IEEE Trans. Biomed. Eng. **46**(2), 213–225 (1999).
[14] Clements, L. W., Chapman, W. C., Dawant, B. M., Galloway, R. L. and Miga, M. I., "Robust surface registration using salient anatomical features for image-guided liver surgery: algorithm and validation," Med. Phys. **35**(6), 2528–2540 (2008).